International Journal of Fracture **70:** 99–115, 1995.

An inelastic multiple discrete asperities model for the effects of compressive underloads in fatigue crack growth

G.A. KARDOMATEAS and R.L. CARLSON
School of Aerospace Engineering, Georgia Institute of Technology, Atlanta, Georgia 30332-0150, USA

Received 27 April 1994; accepted in revised form 21 October 1994

Abstract. As a common practice, the compressive (negative load ratio) excursions are ignored when analyses of fatigue crack growth in metals are conducted. However, recent experimental data on fatigue crack growth with intermittent compressive load excursions have shown that the use of this assumption leads in most cases to nonconservative predictions. This paper presents a model that is capable of explaining the observed behavior, including the 'saturation' of the compressive overload effects, and the increase in the crack growth rate once the initial, positive load ratio profile is resumed, following a compressive excursion. The model is based on the plastic crushing of a single asperity or multiple asperities located on the crack face close to the crack tip and under dominantly plane strain conditions. A comparison of the behavior for one and for two asperities is made. Moreover, the effects of hardness and strain hardening are also examined.

1. Introduction

A common feature of many of the service load spectra is the presence of intermittent compressive excursions. The common analytical practice has been to exclude the compression segments since it seems reasonable to believe that no contribution to crack growth is developed during a compressive excursion, e.g. Bucci [1]. Thus, for a negative load ratio R cycle, the stress intensity factor range is set equal to the maximum stress intensity factor.

A number of experimental programs during the past several years have focused on the effects of compressive load excursions on both smooth bars and cracked specimens. A review of the results from these investigations can be found in Carlson and Kardomateas [2]. A common conclusion of these studies was that the use of the foregoing assumption of neglecting the compressive segment leads to nonconservative predictions. For example, Zaiken and Ritchie [3] observed crack growth below the threshold stress intensity range after the application of large compression overloads.

Kemper et al. [4] have suggested that microstructural features and deformation characteristics influence the observed behavior. They also showed that the type of response observed varied significantly for three metals with different properties. In particular, it was noted that the relative roughness of the fracture surfaces is dependent on microstructure and deformation characteristics. Of the metals tested, in the alloy IN-905 XL the crack surfaces were very flat, so closure obstruction was minimal. In copper, although the fracture surfaces were not flat, closure obstruction appeared to be eliminated when sufficiently high compressive loads were applied. This suggests that the effective heights of the asperities could have been reduced by inelastic deformation.

Both Kemper et al. [4] and Tack and Beevers [5] observed a saturation effect, in which increases in compressive load beyond a certain level did not result in additional increases in

the crack growth rate. This behavior may be a consequence of occurrences either in front or behind the crack tip. Reduction of asperity heights could reasonably be subject to a limiting inelastic deformation. Another influence may come from cyclic strain hardening or softening of the material in front of the crack tip. This could result in either reductions or increases in the size of the cyclic plastic zone.

In another recent work [6], data were obtained on crack growth in tests with an initially positive load ratio $R = 0.1$; the tests were then interrupted, and although the maximum stress was maintained, the minimum stress was reduced to a negative, compressive value, so that a negative $R = -2$ loading was in place. After an interval, the initial, positive $R = 0.1$ loading was resumed. An examination of the data for one of the three alloys tested, namely the Waspaloy, reveals that the rate of crack growth (the slope of the crack extension a versus number of cycles N curve) is discontinuous at each change in loading condition and that the rate of growth of the $R = -2$ segment is substantially greater than that for $R = 0.1$. Another issue, perhaps of secondary importance, is that the final slope of the initial $R = 0.1$ phase is slightly greater than the initial slope of the final $R = 0.1$ segment, which suggests that the interposed $R = -2$ segment may have introduced a transient retardation behavior upon resumption of the $R = 0.1$ loading. Nevertheless, the final slope of the final $R = 0.1$ segment is greater than the final slope of the initial $R = 0.1$ phase, which indicates that the end result of the compressive excursion was an acceleration of growth when the initial load profile was resumed. Some of the results from [6] were also included in [2]. These retardation transients should be the subject of additional investigation. They may, for example, be the result of a transitional change in the mode of closure obstruction. McEvily and Yang [7] observed transitional mode changes, for example, in single and block tensile overload tests.

In another study, Yu et al. [8] presented crack growth test results on the aluminum alloy 2024-T351 in the near threshold region. They found that crack growth curves shifted to lower threshold values and greater crack growth rates as the minimum stress became more compressive. Furthermore, they examined the effects of single, intermittent compressive excursions in tests which were otherwise loaded under fixed positive load ratio R values. Introduction of the compressive cycles substantially shifted the growth rate curves towards higher values.

The closure obstruction effect of a plastic wake generated as a crack advances was analyzed by Budiansky and Hutchinson [9]. They used a Dugdale strip model as a basis for their analysis and demonstrated that a wake in the form of a plastic layer could obstruct closure and therefore reduce the effective range of the stress intensity factor. Budiansky and Hutchinson [9] considered the case of plane stress. Subsequently, Newman [10] extended the use of a Dugdale strip model by introducing a crack advance criterion and treating the plane strain case.

Dugdale strip models result in the production of plastic layers which are in continuous contact along the crack faces. Tack and Beevers [5], however, have presented micrographic evidence that gaps remain between crack faces even under compressive loading. Also, Buck et al. [11] used acoustic wave techniques to show that crack face contact occurs at discrete points. These observations suggest that a discrete asperity model for closure can be useful in diagnosing the mechanics of closure obstruction.

With regard to compressive load excursions, it is reasonable to expect that the height of individual asperities can be reduced by crushing whereas the compressive loading would be less effective in reducing the height of a continous layer for the plain strain case. The crushing

of closure obstacles would qualitatively explain the observations of increased crack growth rate following compressive excursions [4, 8].

In a fundamental paper, Forsyth [12] suggested that the topography of a fracture surface near the crack tip, as well as the externally applied loads, was important to an understanding of crack advance. Modeling surface features such as asperities which act as obstructions to closure leads to a partitioning of the crack tip stress state into two components, i.e. a component caused by external forces which may be classified as global, and one resulting from asperity contact forces which may be termed local. Since there is a variety of local contact force types that can be developed, different crack tip states are possible.

In the same context, the presence of oxide debris in the crack region was shown by Coffin [13] to result in the wedging open of the crack faces during the high temperature fatigue of Udimet 500. The formation of oxide layers on the fatigue fracture surfaces of steels has also been cited as a primary contributor to crack closure during fatigue crack growth at ambient temperatures [14]. Moreover, recent experimental results obtained by Buck et al. [11] have indicated that the primary crack face contacts which prevent closure are immediately adjacent to the crack tip. The single asperity model is an idealization in which complete closure is prevented at one point near the crack tip [15]. As the external load decreases, and the upper and lower fracture surfaces approach one another, however, it seems likely that additional asperity contacts, more distant from the crack tip, would also develop. A multiple asperity model, again based on the elastic compression of the asperities, was presented by Carlson and Beevers [16].

These discrete asperities models provide a rational explanation of the observed behavior due to closure obstruction in load sequences that involve cycling in tension with a positive load ratio, and involve mostly elastic loading/unloading of the asperities. They would not, however, be able to explain the previously described phenomena that have been observed in compressive excursion experiments. Indeed, for compressive excursions of sizable magnitude, a model accounting for the plastic crushing of the asperities is needed. Hence, this work presents an enhanced formulation for both a single or multiple asperity contact, suitable for the negative load ratio loadings. In this context, Herman et al. [17] and Hertzberg et al. [18] have also attributed the compressive excursion effects to the crushing of asperities in the crack wake.

The model that will be described in this work will demonstrate that positive values of stress intensity can be developed with externally applied compressive forces. Notice that negative values of stress intensity factor have no meaning and the model indicates that it is not, in fact, an issue; instead it shows the way in which the compressive loading should be accounted for. It will also be clearly shown that for compressive excursions, the effective range of stress intensity factor should not be taken as the difference between the maximum stress intensity factor and the so-called opening stress intensity factor. Indeed,as the applied load decreases below the 'opening load' and the asperity height is decreased, the total stress intensity factor (global plus local) can decrease. The effective range of the stress intensity factor would be, therefore, the difference between the maximum value and the value corresponding to the minimum load. This has also been illustrated in [2].

2. Formulation

For the plane strain case, the distribution of the asperities is essentially uniform across the specimen thickness, which suggests the possibility of representing the asperities configuration

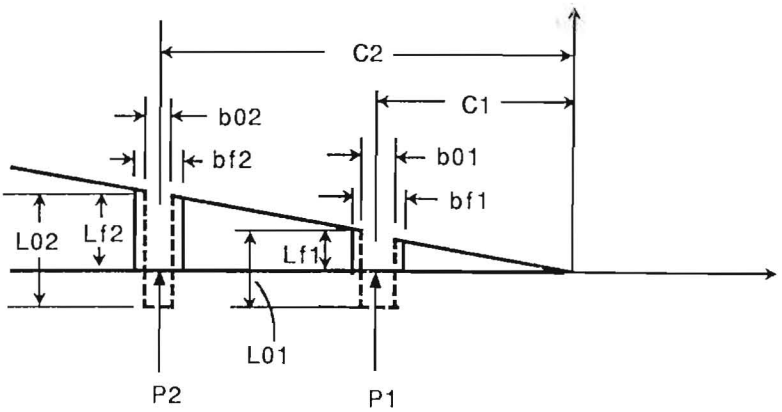

Fig. 1. Multiple asperities on the upper crack face.

through the thickness by an effective (through-thickness) line contact. It should be noted that in the case of oxide build-up on the crack face, the line contact very nearly represents the actual situation [19]. The line contact representation permits the problem to be treated as a two dimensional one.

The essential features of the model are shown in Fig. 1. Only the upper crack face is shown. The distance of kth asperity from the crack tip is C_k. A force P_k develops on each asperity which is in contact. The initial asperity height is L_{0k} and the final, compressed height is L_{fk}. Similarly, the initial asperity width is b_{0k} and the final, compressed, one is b_{0f}. It should be emphasized that asperity spacings are of the order of the grain size in most alloys. Also, Knott [30] has indicated that closure contact may occur at distances of less than 0.1 mm behind the crack tip. Finally, let us denote by t the asperity thickness.

The total mode I stress intensity factor at the crack tip depends on the local crack forces P_k and the external or global loading. The stress intensity factor produced by concentrated, opposing line loads on the crack faces of a semi-infinite crack can be determined from Rice [20]. For a finite center crack of length $2a$, Sih et al. [21] gave corresponding expressions for both mode I and mode II stress intensity factors. The opening mode stress intensity factor for plane strain in terms of the local crack face force is [21]

$$K_{\mathrm{I,local}} = \sum_{k=1}^{n} \left(\frac{1}{\pi C_k}\right)^{1/2} \left(2 - \frac{C_k}{a}\right)^{1/2} \frac{P_k}{t} . \tag{1}$$

This expression is also valid for a single-edge crack of length a (this can be easily shown by following the same procedure as in [21]). Furthermore, if $a \gg c$, this expression reduces to the one for a semi-infinite crack [20].

It should be noted that these expressions for the stress intensity factors produced by a concentrated load on the crack face at a distance C_k behind the tip, given by Sih et al. [21], were for a finite center crack of length $2a$ in an infinite body. This is the reason why these equations do not include the specimen width. Future work would examine the effect of using more accurate expressions by including the specimen width, i.e. by deriving the stress intensity factors produced by a concentrated load on the crack face at a distance C_k behind the tip, for a finite center crack of length $2a$ in a body of width w.

The contribution of the external load will be represented by $K_{\text{I,global}}$. By superposition, the total stress intensity factor is

$$K_I = K_{\text{I,local}} + K_{\text{I,global}} \,. \tag{2}$$

The dimension L_0 represents the initial magnitude of the interference produced by the asperity. The effective initial width of the asperity is b_0 (Fig. 1). Since the asperities may be re-loaded at subsequent cycles after being partially crushed, the $i-$subscript will also be used to denote the current (after the ith cycle) dimensions, e.g. L_{ik} instead of L_{0k}.

The load P will now be determined from a displacement condition at the asperity site, which includes the plastic crushing of the asperity.

The vertical displacement at the upper crack face, i.e. at $\theta = \pi$ and an arbitrary r, is

$$U_2(r, \pi) = U_{2,\text{global}} + U_{2,\text{local}}. \tag{3}$$

By use of the stress intensity factors for the global and the local load, we can write the displacement at the jth asperity site, $r = C_j$, $\theta = \pi$

$$U_2(C_j, \pi) = \frac{2}{G}\left(\frac{C_j}{2\pi}\right)^{1/2}(1-\nu)K_{\text{I,global}} + \sum_{k=1}^{n}\frac{2(1-\nu)}{\pi G}\left(1-\frac{C_k}{2a}\right)^{1/2}\frac{P_k}{t}\,, \tag{4}$$

where G is the shear modulus and ν the Poisson's ratio.

Hence, the first set of conditions for determining the forces P_k is the displacement at each of the asperity sites

$$U_2(C_j, \pi) = L_{fj}\,, \quad j = 1, \ldots, n. \tag{5}$$

Since L_{fj} is not known, let us consider now the relations between the interference heights during closure L_{fk} and asperity forces P_k.

Each asperity is assumed under uniaxial compression σ_k (all other stress components are zero). Moreover, the total equivalent strain of each asperity is

$$\bar{\epsilon}_k^T = \bar{\epsilon}_k^e + \bar{\epsilon}_k^p\,, \tag{6}$$

where $\bar{\epsilon}^e$ is the elastic and $\bar{\epsilon}^p$ the plastic component (we consider positive the asperity stress σ and strain ϵ when they are compressive). Notice that in uniaxial compression, although there are other nonzero components of strain, namely, $\epsilon_{11} = \epsilon_{33} = -\epsilon_{22}/2$, it turns out that $\bar{\epsilon} = \epsilon_{22}$. Hence, since

$$\bar{\epsilon}_k^e = \sigma_k/E\,; \quad \bar{\epsilon}_k^T = \ln\frac{L_{0k}}{L_{fk}}\,, \tag{7}$$

the plastic strain component is

$$\bar{\epsilon}_k^p = \ln\frac{L_{0k}}{L_{fk}} - \frac{\sigma_k}{E}\,, \tag{8}$$

where E is the modulus of elasticity. Assume now an equivalent true stress vs. integrated equivalent plastic strain law

$$\bar{\sigma} = \sigma_0\left(\epsilon_0 + \bar{\epsilon}^p\right)^n\,, \tag{9}$$

where n is the strain hardening exponent. Let us denote by $A_{0k} = tb_{0k}$ the initial cross-sectional area of each asperity. For simplicity, we shall again consider the material as being incompressible in both the elastic and the plastic ranges when cross-sectional area calculations are performed (this would be strictly accurate if the Poisson's ratio is 0.5; however, the error introduced for the usual value of 0.3 can be reasonably expected to be small, if the elastic strains are small compared to the plastic ones). Therefore, using the incompressibility requirement $A_{fk}L_{fk} = A_{0k}L_{0k}$, to obtain a relationship for the current cross-section A_{fk}, and the stress $\sigma = P/A_f$, and subsequently substituting in (7) and (8) gives one equation in P_k, L_{fk}

$$\left[\frac{P_k L_{fk}}{\sigma_0 A_{0k} L_{0k}}\right]^{1/n} = \ln\frac{L_{0k}}{L_{fk}} - \frac{P_k L_{fk}}{EA_{0k}L_{0k}} + \epsilon_0 \,. \tag{10a}$$

If the k-asperity is compressed below yield, then the foregoing equation is replaced with

$$\frac{P_k}{EA_{ik}} = 1 - \frac{L_{fk}}{L_{ik}}\,, \quad k = 1, 2, \ldots n, \tag{10b}$$

where L_{ik}, A_{ik} are the current (after the ith cycle) asperity height and cross-sectional area when the kth asperity is re-loaded.

The other set of equations needed to solve for L_{fk} and P_k is found by combining (4) and (5)

$$L_{fj} = \frac{2}{G}\left(\frac{C_j}{2\pi}\right)^{1/2}(1-\nu)K_{\text{I,global}} + \sum_{k=1}^{n}\frac{2(1-\nu)}{\pi G}\left(1 - \frac{C_k}{2a}\right)^{1/2}\frac{P_k}{t}\,. \tag{11}$$

Notice that the final, crushed asperity width can be found from the volume preservation condition and the transverse strain equality $\epsilon_{11} = \epsilon_{33}$ (if 2 denotes the axial direction)

$$b_{fk} = b_{0k}\sqrt{L_{0k}/L_{fk}}\,. \tag{12}$$

If all asperities are loaded elastically, then eliminating L_{fk} leads to the following system of n linear equations for determining P_k

$$P_k\left[\frac{L_{ik}}{EA_{ik}} + \frac{2(1-\nu)}{G\pi t}\left(1 - \frac{C_k}{2a}\right)^{1/2}\right] + \sum_{j\neq k} P_j \frac{2(1-\nu)}{G\pi t}\left(1 - \frac{C_j}{2a}\right)^{1/2}\left(\frac{C_k}{C_j}\right)^{1/2}$$
$$= L_{ik} - \frac{2(1-\nu)}{G}\left(\frac{C_k}{2\pi}\right)^{1/2} K_{\text{I,global}}\,, \quad k = 1, 2, \ldots n \tag{13}$$

Although any number of asperities can be considered, attention will be confined to a two asperity model. This allows the roles of the model parameters to be easily discerned.

Two asperity model. In the case of two asperities, Eqns. (11) become:

$$\frac{2(1-\nu)}{G\pi t}P_1 + \frac{2(1-\nu)}{G\pi t}\left(\frac{C_1}{C_2}\right)^{1/2} P_2 = L_{f1} - \frac{2(1-\nu)}{G}\left(\frac{C_1}{2\pi}\right)^{1/2} K_{\text{I,global}}\,, \tag{14a}$$

$$\frac{2(1-\nu)}{G\pi t}\left(\frac{C_2}{C_1}\right)^{1/2} P_1 + \frac{2(1-\nu)}{G\pi t}P_2 = L_{f2} - \frac{2(1-\nu)}{G}\left(\frac{C_2}{2\pi}\right)^{1/2} K_{\text{I,global}}\,. \tag{14b}$$

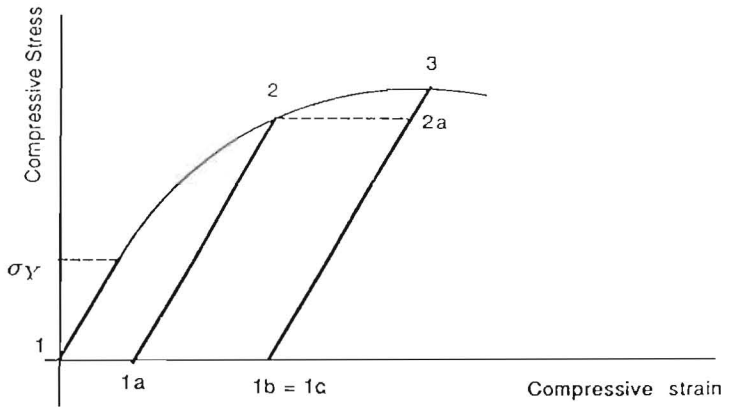

Fig. 2. Schematic of asperity loading/unloading behavior.

Since in this system of two linear equations in P_1, P_2, the determinant of the coefficients of the P_k's is zero, a solution is possible only if both the determinants with the constant columns are also zero. This requirement results in the following single relationship between the compressed asperity heights

$$L_{f1} = \left(\frac{C_1}{C_2}\right)^{1/2} L_{f2}\,. \tag{15}$$

The description of the asperity behavior for the two separate phases, i.e. the loading and unloading one, will follow next, by reference to Fig. 2.

Loading phase. During the application of the external cyclic load, Q, asperity loading may occur from the initial configuration or it may involve re-loading after the asperity has been plastically crushed to a reduced height. Hence, during the decreasing external load cycle (loading the asperity) from a general position (Q_i, $P_{ik} = 0$, L_{ik}, A_{ik}) to a position ($Q_f < Q_i$, P_k, $L_{fk} \leqslant L_{ik}$, $A_{fk} \geqslant A_{ik}$) the following conditions may develop:

(a) No contact takes place for both asperities and $K_I = K_{I,global}$ if, from (11):

$$\frac{2(1-\nu)}{G}\left(\frac{C_j}{2\pi}\right)^{1/2} K_{I,global} > L_{ij}\;;\quad j = 1,2. \tag{16}$$

(b) Only the first asperity is in contact. From (11), this occurs if

$$\frac{2(1-\nu)}{G}\left(\frac{C_2}{2\pi}\right)^{1/2} K_{I,global} + \frac{2(1-\nu)}{G}\left(\frac{C_2}{2\pi}\right)^{1/2}\left(\frac{2}{C_1\pi}\right)^{1/2}\frac{P_1}{t} > L_{i2}; \tag{17}$$

Then a single asperity analysis can be performed and give the load of the first asperity P_1, and the local stress intensity factor.

(c) In a similar fashion, only the second asperity may be in contact.

(d) If the foregoing conditions are not met, and contact of both asperities takes place, the following numerical solution procedure is followed: for a specific L_{f2}, P_2 is determined so that the constitutive of the second asperity (either elastic or plastic) is satisfied. Subsequently, L_{f1} is found from (15), i.e. $L_{f1} = L_{f2}\sqrt{C_1/C_2}$, and P_1 is determined so that the constitutive of the first asperity (either elastic or plastic) is satisfied. Finally, iterate through values of L_{f2} so that L_{f1} and P_1 so determined satisfy the displacement condition, (14a).

In each of the previous steps, to determine the force P_k that corresponds to a final asperity height L_{fk}, first examine if elastic compression take place. This would occur if

$$P_k = EA_{ik}\left(1 - \frac{L_{fk}}{L_{ik}}\right) < P_u \ , \tag{18}$$

where P_u is the load from which the asperity was unloaded, or the yield load if no previous plastic loading was involved. If the relation (18) is not satisfied, then the plastic constitutive equation (10a) is numerically solved; the search starts from the elastic limit, i.e. with $L_{\min} = L_i - P_u L_i/(EA_i)$.

In all cases, the local stress intensity factor is given in terms of the asperities loads P_k by (1) and the total (global and local) stress intensity factor by (2). Notice again that the current asperity heights L_{ik} and cross-sectional area A_{ik} are sometimes needed instead of the initial values L_0 and A_0 respectively, since on re-loading after a compressive excursion, the asperity is loaded elastically from the current (crushed asperity) dimensions.

Unloading phase. During the increasing external load cycle (unloading the asperity to zero asperity load, e.g. 2-1a or 3-1c in Fig. 2), from a position (Q_f, P_{uk}, L_{fk}, A_{fk}) to a position ($Q_{ik} > Q_{fk}$, $P_k = 0$, $L_{ik} > L_{fk}$, $A_{ik} < A_{fk}$), we recover not the initial asperity heights L_{0k}, but the final compressed ones, L_{fk}, plus the changes in height that are given by the elastic solution that corresponds to the loads P_{uk} at which unloading of each asperity takes place, i.e.

$$L_{ik} = L_{fk} + \frac{P_{uk}L_{fk}}{EA_{fk}} \ ; \quad A_{ik} = L_{0k}A_{0k}/L_{ik} \ . \tag{19}$$

Notice that L_{ik} are now the 'new' (after unloading) interference heights.

Moreover, we do not recover the initial cross-sectional area and asperity width, but the final, crushed asperity ones minus the elastic recovery, which can again be found by use of (19).

An important point of this analysis will now be discussed. Since the crack will always be open due to the asperity interference, during the compressive segment of the applied load cycle, i.e. when $Q < 0$, there is a negative contribution of the external load to the stress intensity factor, i.e. $K_{\text{I,global}}$ has a negative sign and it is calculated by the same relation as for a positive external load. An analogous way to envision this is to consider the same single-edge cracked configuration when an opening tensile loading Q is first applied, and then a closing bending moment M is applied (Fig. 3). A pure bending moment M, applied alone, would result in zero stress intensity $K = K_M = 0$. On the contrary, a pure tensile load, applied alone, would give a nonzero $K = K_Q > 0$. The combined case, however, would have a stress intensity $K = K_Q - K_M > 0$, i.e., it would entail a *'negative' contribution* of the closing bending moment M. Hence, a 'negative K' can contribute, *if the crack is open.*

3. Application of the model

The model described in the previous section has been used to analyze the responses due to increasing magnitudes of compressive underloads and also to study the effects of hardness and strain hardening.

Consider a metal with the mechanical properties (baseline material): $E = 200$ GN/m^2, $\nu = 0.3$, yield strength $\sigma_y = 400$ MN/m^2, strain-hardening exponent $n = 0.30$ and the constant of (9), $\sigma_0 = 700$ MN/m^2. The other constant in the relation (9) that describes the behavior

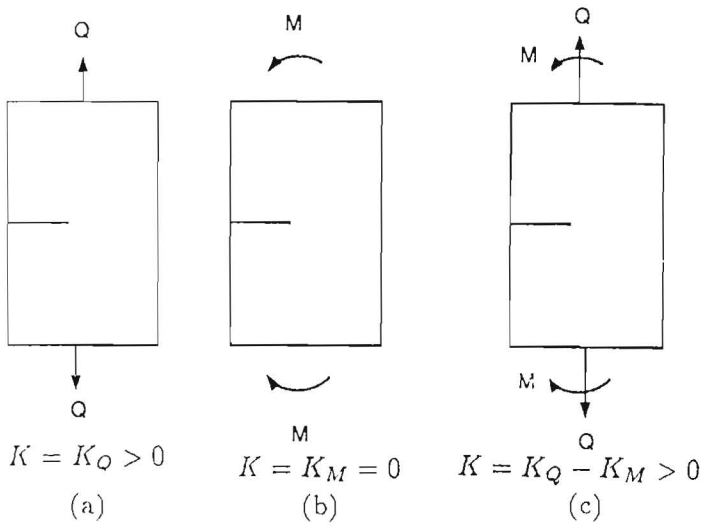

Fig. 3. Illustrating the negative contribution of a closing bending moment on the stress intensity factor: (a) pure tension, (b) pure bending, and (c) combined tension and bending.

beyond yield is found by fitting the yield point, i.e. $\epsilon_0 = (\sigma_y/\sigma_0)^{1/n}$. These material constants are typical of a hot rolled steel. A single-edge-cracked specimen of thickness $t = 13$ mm and width $w = 26$ mm with a crack of length $a = 11$ mm is assumed.

For this case of single-edge through crack of length a in a plate of width w under a remote normal load Q, the stress intensity factor is, e.g. [22]

$$K_{\mathrm{I}}(Q) = \frac{Q}{wt}\sqrt{\pi a}\left(1.12 - 0.23\frac{a}{w} + 10.6\frac{a^2}{w^2} - 21.7\frac{a^3}{w^3} + 30.4\frac{a^4}{w^4}\right) . \tag{20}$$

Consider first a single asperity configuration with an initial interference height $L_0 = 20\ \mu$m and initial width $b_0 = 50\ \mu$m. The distance from the crack tip is $C = 15\ \mu$m. These are typical dimensions of experimentally observed asperities as reported in [15]. First, the opening load (load at which asperity contact is established), Q_{OP}, is found by setting $P = 0$ in (11b)

$$K_{OP} = \frac{L_0 G}{2(1-\nu)}\left(\frac{C}{2\pi}\right)^{-1/2} = K_{\mathrm{I}}(Q_{OP}) . \tag{21}$$

The effect of an increasing compressive underload (Fig. 4a) on the opening stress intensity factor is shown in Fig. 4b, in a plot of the ratio of K_{OP} (after the compressive excursion) to the initial $K_{OP} \equiv K_{OP}^{(0)}$, versus the ratio of the compressive underload to the initial opening load. This plot clearly explains and quantifies the experimentally observed phenomena:

(i) due to the decreasing K_{OP}, and hence the increasing ΔK, the crack growth rate increases following a compressive excursion, and

(ii) the 'saturation' of compressive underload effects (no further change in ΔK after sufficiently large underloads).

Strain hardening effects are presented in Table 1 for two model materials, namely the baseline material and a low-hardening one with the same yield strength $\sigma_y = 400$ MN/m^2, strain-hardening exponent $n = 0.10$ and $\sigma_0 = 500$ MN/m^2. The opening stress intensity factor K_{OP} is uniformly lower for the low hardening case with the difference in the value of K_{OP} for the two materials of the order of 13 percent.

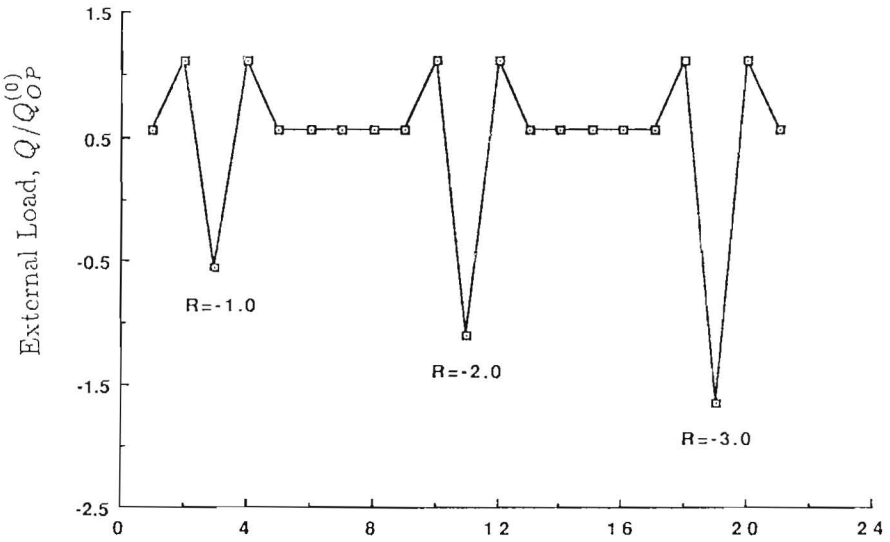

(a)

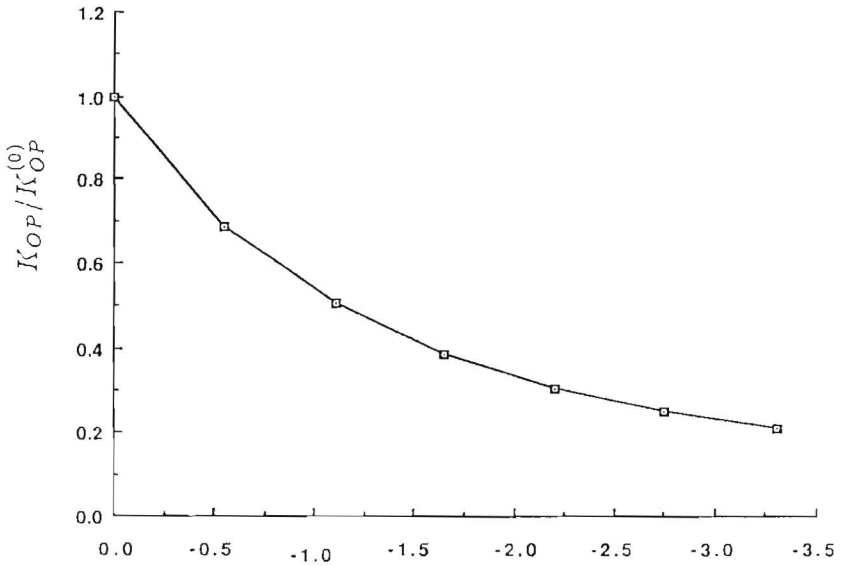

(b)

Fig. 4. (a) A sequence of increasing compressive excursions. $Q_{OP}^{(0)}$ is the opening (or closure) load that corresponds to the initial state, i.e. when no compressive excursions have been applied. (b) The opening stress intensity factor K_{OP} versus the compressive excursion Q from Fig. 4a for the single asperity model; $K_{OP}^{(0)}$ and $Q_{OP}^{(0)}$ are the opening stress intensity factor and the opening (or closure) load that correspond to the initial state, i.e. when no compressive excursions have been applied.

The effect of material hardness has been examined by use of two model materials, namely the baseline material and a 'hard' one with yield strength σ_y = 600 MN/m^2 and the same strain-hardening exponent n = 0.30 and σ_0 = 700 MN/m^2. Again, Table 1 shows the effect of

Table 1. $K_{OP}/K_{OP}^{(0)}$ after applying a compressive excursion of magnitude Q. Single asperity: initial interference height, $L_0 = 20$ μm; initial width $b_0 = 50$ μm

	At a distance from the crack tip: $C = 15$ μm		
Q/Q_{OP}	Baseline	Low-hardening†	'Hard'†
	$n = 0.3$, $\sigma_0 = 700$ MPa, $\sigma_y = 400$ MPa,	$n = 0.1$, $\sigma_0 = 500$ MPa, $\sigma_y = 400$ MPa,	$n = 0.3$, $\sigma_0 = 700$ MPa, $\sigma_y = 600$ MPa
0.00	1.00	1.00 (0.0%)	1.00 (0.0%)
−0.55	0.686	0.604 (−12.0%)	0.755 (10.0%)
−1.10	0.505	0.436 (−13.7%)	0.581 (15.0%)
−1.65	0.387	0.333 (−14.0%)	0.459 (18.6%)
−2.20	0.306	0.265 (−13.4%)	0.372 (21.6%)
−2.75	0.250	0.217 (−13.2%)	0.310 (24.0%)
−3.30	0.209	0.183 (−12.4%)	0.263 (25.8%)

† Quantities in parentheses are percentage differences from baseline.

material hardness by giving the values of the opening stress intensity factor K_{OP}. These are found to be higher for the 'hard' material, with the difference in the value of K_{OP} for the two materials uniformly increasing with the value of the applied underload.

Two-asperity configuration. Consider now a two-asperity case, where, in addition to the asperity described before (asperity 1), a second asperity of (slightly larger) initial height $L_0 = 25$ μm and the same initial width exists at a distance $C_2 = 20$ μm.

First the opening load is found from the load to touch either asperity, i.e.

$$K_{OP} = \max\left\{ \frac{L_{01}G}{2(1-\nu)}\left(\frac{C_1}{2\pi}\right)^{-1/2}, \quad \frac{L_{02}G}{2(1-\nu)}\left(\frac{C_2}{2\pi}\right)^{-1/2} \right\} = K_I(Q_{OP}) . \tag{22}$$

Now consider the two-asperity configuration when a load sequence as shown in Fig. 5 is applied. First, the specimen is cycled between $1.1Q_{OP}$ and $0.55Q_{OP}$, so that the load ratio is positive, $R = 0.5$. Then a compressive excursion to $-2.2Q_{OP}$, i.e, a negative $R = -2$, is applied. Subequently, the initial, positive $R = 0.5$ is resumed. Then, a second compressive excursion of the same end points, $R = -2$, is applied. Finally, the initial, positive $R = 0.5$ load profile is resumed for the third time.

Figures 6a,b show the two asperity interference heights L_{i1}, L_{i2} and Fig. 6c the local stress intensity factor K_{IIocal} at the different stages of this loading sequence. At the first $R = 0.5$ load segment, the asperities are cycled with very small elastic changes in height, which is completely recovered at the end of each cycle. A sizable K_{IIocal} is developed at the end of each asperity loading (specimen unloading) cycle.

During the compressive excursion, however, the asperities are plastically crushed to about 60 percent of their original height and a much larger K_{IIocal} is developed at the minimum (compressive) load. Very little elastic unloading of the asperities takes place at the positive, maximum load.

Once the initial, positive $R = 0.5$ is resumed, the asperities have been adequately crushed, so that no contact is established and therefore, a zero K_{IIocal} is developed. During the second

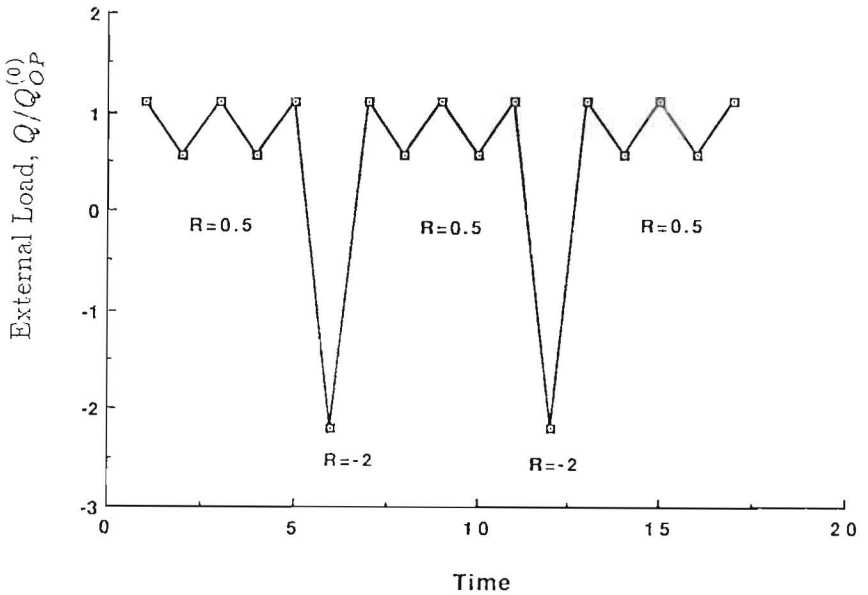

Fig. 5. Another example of an applied load sequence. Again, $Q_{OP}^{(0)}$ is the opening (or closure) load that corresponds to the initial state, i.e. when no compressive excursions have been applied.

compressive $R = -2$ excursion, the asperities are again plastically crushed and their height is reduced further to about 35% of their original value, whereas the K_{IIocal} that develops at the minimum point is somewhat smaller than in the first compressive excursion. On resuming the initial, positive $R = 0.5$ load profile for the third time, again no asperity contact is occurring, and $K_{\text{IIocal}} = 0$. Notice that during this load sequence, the cross-sectional area of the asperity would tend in the inverse manner, i.e. increasing when the asperity height is decreasing.

It should also be noted that in general, due to strain hardening effects and increases in the asperity cross-sectional area, successive underload cycling may not lead to successive noticeable decreases in asperity height. Also, as the crack grows, additional underloading will have new, increased values of C_k, and this also would lead to a reduced plastic crushing of the asperity.

The quantity that controls the fatigue crack growth rate is the range in the total stress intensity factor ΔK. Figure 7 shows the total stress intensity factor at the different stages of the loading sequence. In all segments, at the maxiumum positive external load, $K = K_{\text{Iglobal}}$ and the range ΔK is affected by the minimum (positive or negative) external load, at which asperity contact may develop, and a nonzero K_{IIocal} may be generated. At the first $R = 0.5$ load segment, ΔK is relatively small (because of the rather large K_{IIocal} at the load minimum).

During the compressive excursion, which crushes the asperities, ΔK is increased substantially. Notice that at the minimum, negative load point, K is positive, nonzero. Once the positive $R = 0.5$ is resumed for the second time, ΔK is larger than in the initial $R = 0.5$ load segment (because now no asperity contact takes place). During the second compressive $R = -2$ excursion, which again crushes further the asperities, ΔK is again increased to a value beyond that in the first $R = -2$ segment. On resuming the positive $R = 0.5$ load profile for the third time, again no asperity contact takes place, and ΔK is larger than in the initial $R = 0.5$ load segment, but no different than the second $R = 0.5$ load segment. Therefore, this model provides an explanation for the following experimentally observed phenomena:

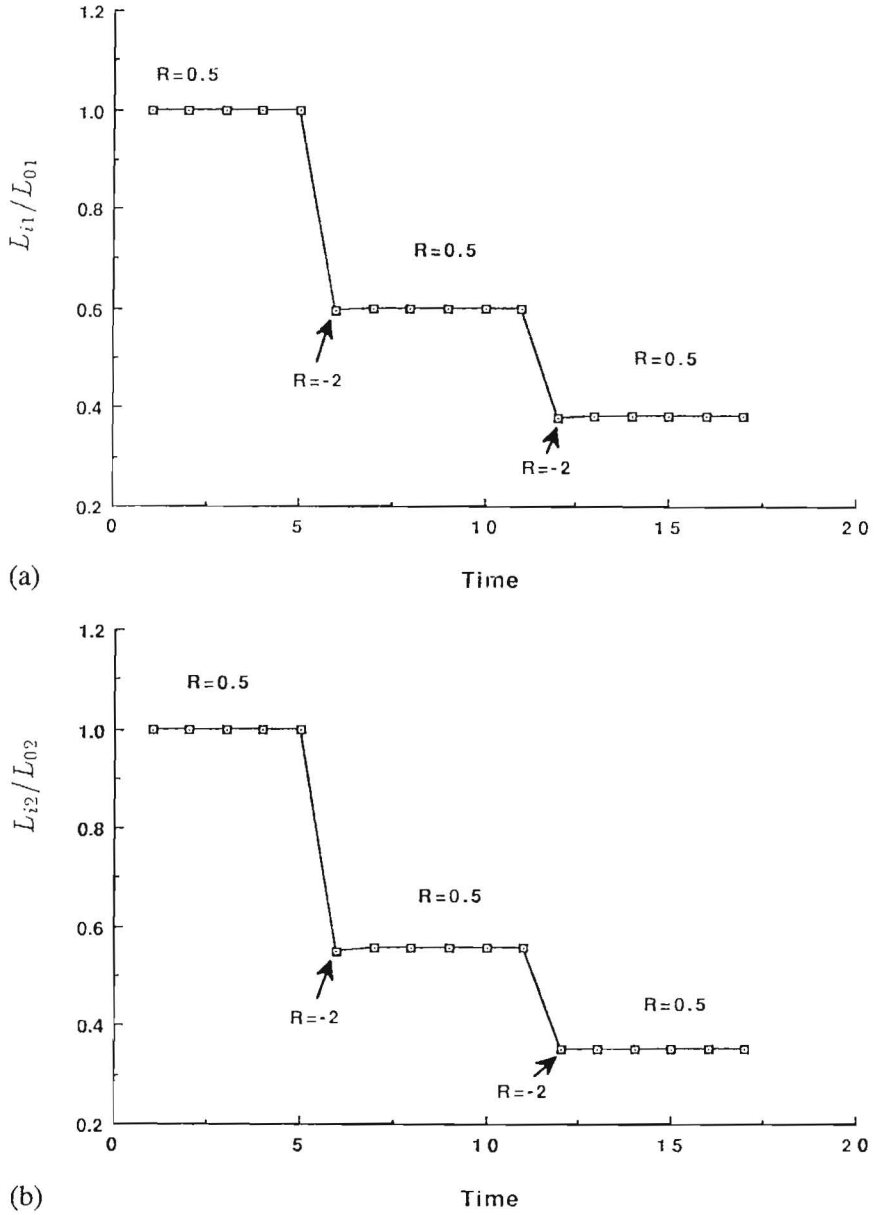

Fig. 6. (a) First (closest to the crack tip) asperity height at different moments during the application of the load sequence of Fig. 5. (b) Second (furthest from the crack tip) asperity height at different moments during the application of the load sequence of Fig. 5.

(a) increase in crack growth rate following a compressive excursion (increase in ΔK), and
(b) the 'saturation' of compressive underload effects (no further change in ΔK).

4. Discussion

For the external maximum loads applied, it can be expected that small plastic enclaves would form at the crack tip. Since this can result in a relaxation of the stress state at the crack tip,

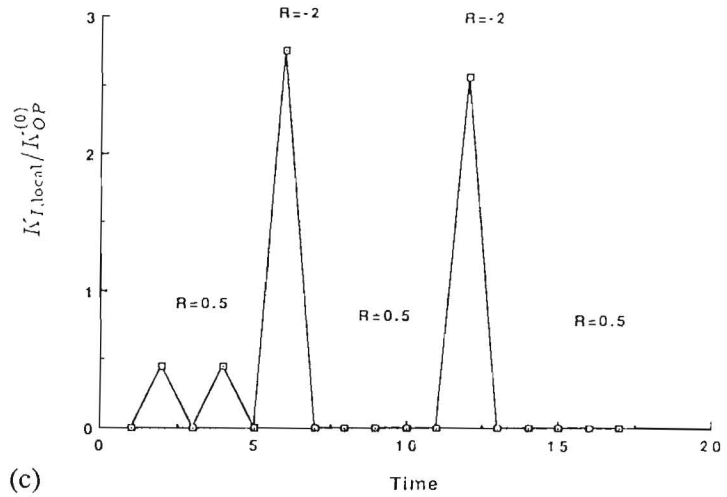

Fig. 6 (Cont.)

(c) The local stress intensity factor corresponding to the load sequence in Fig. 5. $K_{OP}^{(0)}$ is the opening stress intensity factor that corresponds to the initial state, i.e. when no compressive excursions have been applied.

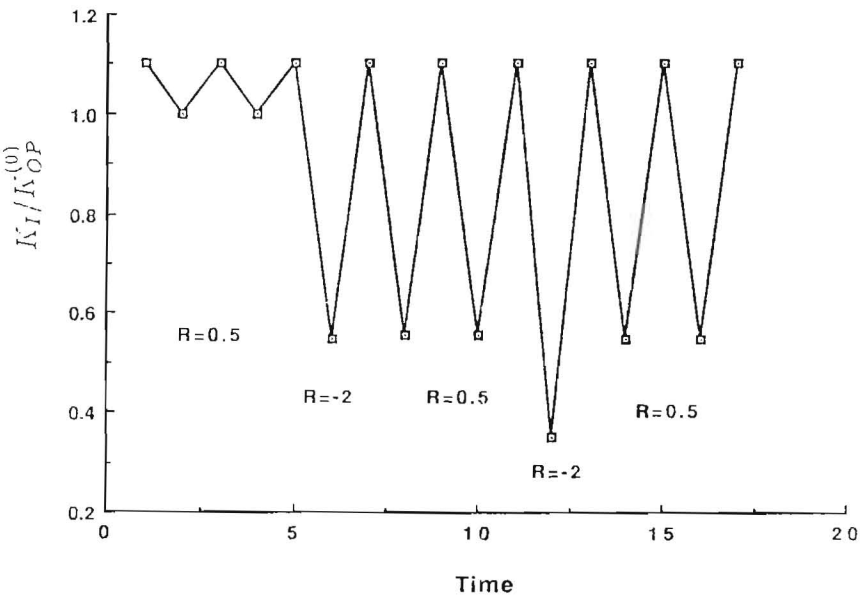

Fig. 7. The total stress intensity factor at different moments during the application of the load sequence of Fig. 5 for the two-asperity model. Again, $K_{OP}^{(0)}$ is the opening stress intensity factor that corresponds to the initial state, i.e. when no compressive excursions have been applied.

an estimate of the magnitude of this effect was made. Irwin [23] has proposed the concept of an effective crack length, by adding half of the plastic zone size. This concept was applied to increase the distance from the crack tip to the asperity. Thus, C was increased by $\frac{1}{2}$ of the plastic zone. For plane strain, an estimate of this quantity is [24]

$$R_p = \frac{1}{6\pi}\left(\frac{K_{\max}}{\sigma_y}\right)^2 . \tag{23}$$

Assuming a single asperity configuration at $C = 15\ \mu$m, with an initial interference height of $L_0 = 25\mu$m for the baseline material and carrying out the analysis by substituting $(C + R_p)$ in place of C, gives for the applied load sequence of Fig. 5, lower minimum K_I values for both the initial $R = 0.5$ segment and the compressive $R = -2$ excursion, and hence higher corresponding ΔK values. The subsequently resumed second $R = 0.5$ segment would not be affected, because it turns out that no asperity contact takes place during this segment. Hence, the inclusion of this correction would tend to accelerate the growth at the compressive phase, but diminish the growth acceleration of the second positive load ratio phase relative to the first one, as well as that of the compressive excursion segment relative to the initial positive load ratio phase.

It is also interesting to examine the effect of including the plasticity effects in the asperity deformation on the zero load stress intensity factor, K_{I0}. For completely elastic behavior, at $K_{I,global} = 0$, (13) and (1) give for the same single asperity configuration

$$K_{I0,elastic} = K_{I,local} = \left(\frac{2}{\pi C}\right)^{1/2} \left[\frac{1}{Eb} + \frac{2(1-\nu)}{\pi G L_0}\left(1 - \frac{C}{2a}\right)^{1/2}\right]^{-1} . \tag{24}$$

For the example configuration considered previously, (24) would result in a $K_{I0,elastic}$ only 0.5 percent less than the opening value, K_{OP}. However, inclusion of the plasticity effects would predict that the zero load value of the stress intensity, $K_{I0,plastic}$, is 22 percent less than K_{OP}.

In addition to this tip plasticity effect, one other factor that should be included in analyzing compressive underloads, is that the possible intervening crack extension during the compressive excursion phase would tend to increase the growth acceleration of the second positive load ratio phase relative to the first one. Therefore, this crack extension would produce a contribution which opposes the tip plasticity effect.

Although the present model has a unique capacity in explaining the observed behavior when compressive excursions are part of a spectrum loading, it is not the only attempt to examine this subject. A scheme for including the effects of the compressive load excursions has been proposed by Chang et al. [25]. They introduced a complex empirical procedure which reduces the plastic zone size used in the Willenborg model [26].

A rational explanation for a Willenborg-type mechanism in the context of compressive excursions may be described by reference to Fig. 8. The analytical assumption that the crack surfaces are perfectly flat is represented in Fig. 8a. A uniformly applied compression can be reasonably expected to produce a uniform, compressive stress state in such a cracked body. The body in Fig. 8b is, however, more representative of what is actually encountered. The void shown adjacent to the crack tip represents a gap of the type seen in micrographs. Tack and Beevers [5], for example, observed that even under maximum compressive loading, complete closure did not occur. When the presence of such a void is recognized, it follows that the local stress will not be a simple, uniform compression. It could, in fact, result in a very large effective, compressive stress concentration. A very large compressive stress could produce localized compressive yielding. Upon unloading, there would then be a tensile residual stress in front of the crack tip. The tensile residual stress would be superimposed on the stresses produced by the externally applied load.

This mechanism is analogous to that which has been used in experiments designed to initiate cracks. Suresh and Brockenbrough [27] and Tack and Beevers [5] have applied compressive loads to notched specimens to generate residual tensile stress fields which increase the total

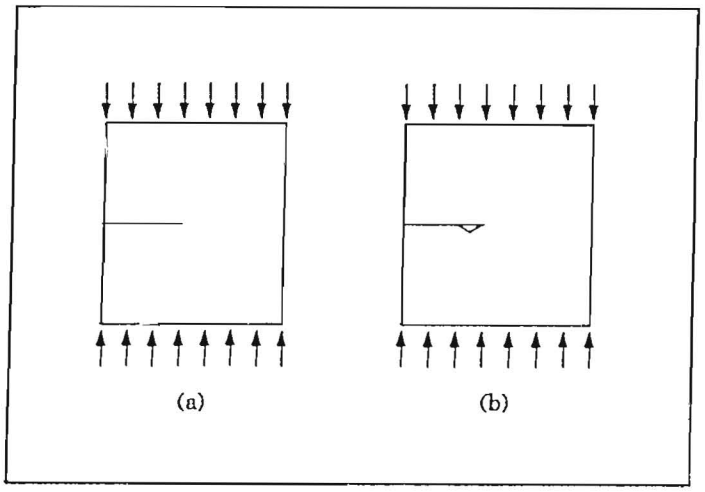

Fig. 8. A compressed crack with the presence of an adjacent void.

sensitivity to crack initiation under subsequent cyclic loading. The scales (micro versus macro) for these examples are different, but the mechanisms are similar.

The Willenborg model introduces an effective stress intensity factor which accounts for the presence of a residual stress state. Specifically, for a tensile overload, an effective stress intensity factor K_{eff} is defined as

$$K_{\text{eff}} = K - K_R \,, \tag{25a}$$

where K_R is the residual stress intensity factor. For a compressive overload, a change in the sign of the residual stress is formally accounted for, by the definition

$$K_{\text{eff}} = K + K_R \,. \tag{25b}$$

However, in this approach, no change occurs for the range of the stress intensity factor ΔK but the effective stress ratio would be of the form

$$R_{\text{eff}} = (K_{\min} + K_R)/(K_{\max} + K_R) \,. \tag{25c}$$

It should be noted that the K_R of the Willenborg model is not the result of a solution to a mechanics problem, but a rationally evolved, non-unique result as discussed in Carlson et al. [28]. Also, the above definition of R_{eff} does not account for the effects due to closure obstruction. It can be expected that both closure and residual stresses may be present for some loading conditions, particularly in the near threshold region.

The model discussed in this paper is based on a mechanism that would affect the effective range of the mode I stress intensity factor. The local loads developed between impinging fracture surfaces are not, however, exclusively restricted to mode I effects. Micrographs of fracture surfaces reveal inclined jogs or steps along the crack path. Furthermore, one of the consequences of the misfit developed between the surfaces of growing cracks is the development of contact friction. As has been discussed in [2], although the latter may be insignificant for tension-tension tests, they could be important for tests with compressive excursions.

Finally, the proposed model may be capable of explaining one additional experimentally observed phenomenon. On specimen loading (unloading the asperities), if the asperities weld

to one another, then a tensile force will be developed in the asperities. This would result in a further reduction in the range of the stress intensity factor. This mechanism may account for the differences in growth rates between tests in an inert atmoshpere, where welding can occur, and an active atmosphere where welding does not occur [29].

Acknowledgements

The authors acknowledge that the studies which led to the preparation of this paper were initiated during the support of the Warner Robins Air Logistics Center, Robins AFB under Contract No: F09603-91-G-0096-0013. They are grateful for the interest and encouragement provided by the Project Monitor, Mr. Gary Chamberlain.

References

1. R. Bucci, *ASTM STP 738* (1981) 5–28.
2. R.L. Carlson and G.A. Kardomateas, *International Journal of Fatigue* 16 (1994) 141–146.
3. E. Zaiken and R.O. Ritchie, *Engineering Fracture Mechanics* 22 (1985) 35–48.
4. H. Kemper, B. Weiss and R. Stickler, *Engineering Fracture Mechanics* 32 (1989) 591–600.
5. A.J. Tack and C.J. Beevers, *Proceedings, Fourth International Conference on Fatigue and Fatigue Thresholds*, Honolulu, 15–20 July 1990, MCPE Ltd, UK (1990) 1179–1184.
6. R.L. Carlson, E. Blakeley, G.A. Kardomateas and C.J. Beevers, *Proceedings, Fifth International Conference on Fatigue and Fatigue Thresholds*, Montreal, 3–7 May 1993, MCPE Ltd, UK (1993) 877–822.
7. A.J. McEvily and Z. Yang, *Proceedings, Fourth International Conference on Fatigue and Fatigue Thresholds*, Honolulu, 15–20 July 1990, MCPE Ltd, UK (1990) 23–36.
8. M.T. Yu , T.H. Topper and P. Au, *Proceedings, Second International Conference on Fatigue and Fatigue Thresholds*, Birmingham, 3–7 September 1984, Chameleon Press, UK (1984) 179–190.
9. B. Budiansky and J.W. Hutchinson, *ASME Journal of Applied Mechanics* 45 (1978) 267–276.
10. J.C. Newman, Jr., *ASTM STP 748* (1981) 53–84.
11. O. Buck, R. Thompson and D. Rehbein, *ASTM STP 982* (1988) 536–547.
12. P.J.E. Forsyth, *International Journal of Fatigue* (1983) 3–14.
13. L.F. Coffin, *Proceedings of the Institute of Mechanical Engineers* 188 (1974) 109–127.
14. S. Suresh, G.F. Zamiski and R.O. Ritchie, *Metallurgical Transactions* 12A (1981) 1435–1443.
15. C.J. Beevers, R.L. Carlson, K. Bell and E.A. Starke, *Engineering Fracture Mechanics* 19 (1984) 93–100.
16. R.L. Carlson and C.J. Beevers, *Engineering Fracture Mechanics* 20 (1984) 687–690.
17. W.A. Herman, R.W. Hertzberg and R. Jaccard, in *Advances in Fracture Research, 7th International Conference on Fracture*, vol. 2, Houston, TX, Pergamon, Oxford (1989) 1417.
18. R.W. Hertzberg, W.A. Herman, T. Clark and R. Jaccard, *ASTM STP 1149* (1992) 197–220.
19. C.M. Ward-Close and C.J. Beevers, *Metallurgical Transactions* 12A (1980) 1435–1443.
20. J.R. Rice, in *Fracture of Solids*, vol. 2, H. Liebowitz (ed.), Academic Press, New York (1969) 218–221.
21. G.C. Sih, P.C. Paris and F. Erdogan, *ASME Journal of Applied Mechanics* (1962) 306–312.
22. K. Hellan, *Introduction to Fracture Mechanics*, McGraw-Hill, New York (1984).
23. G.R. Irwin, *Proceedings, Seventh Sagamore Ordnance Materials Research Conference* (August 1960).
24. F.A. McClintock and G.R. Irwin, *ASTM STP 381* (1965) 84–113.
25. J.B. Chang, M. Szamossi and L-W. Liu, *ASTM STP 748* (1981) 115–132.
26. J. Willenborg , R. Engle and H. Wood, Report AFFDL-TM-71-1 (1971).
27. S. Suresh and J.R. Brockenbrough, *Acta Metallurgica* 36 (1988) 1455–1470.
28. R.L. Carlson, G.A. Kardomateas and P.R. Bates, *International Journal of Fatigue* (1991) 453–460.
29. C.J. Beevers and R.L. Carlson, in *Fatigue Crack Growth – 30 Years of Progress*, R.A. Smith (ed.) Pergamon Press (1986) 89–101.
30. J.F. Knott, in *Fatigue Crack Growth – 30 Years of Progress*, Pergamon, Oxford (1986) 31–52.